DOI: 10.1038/NMAT4359

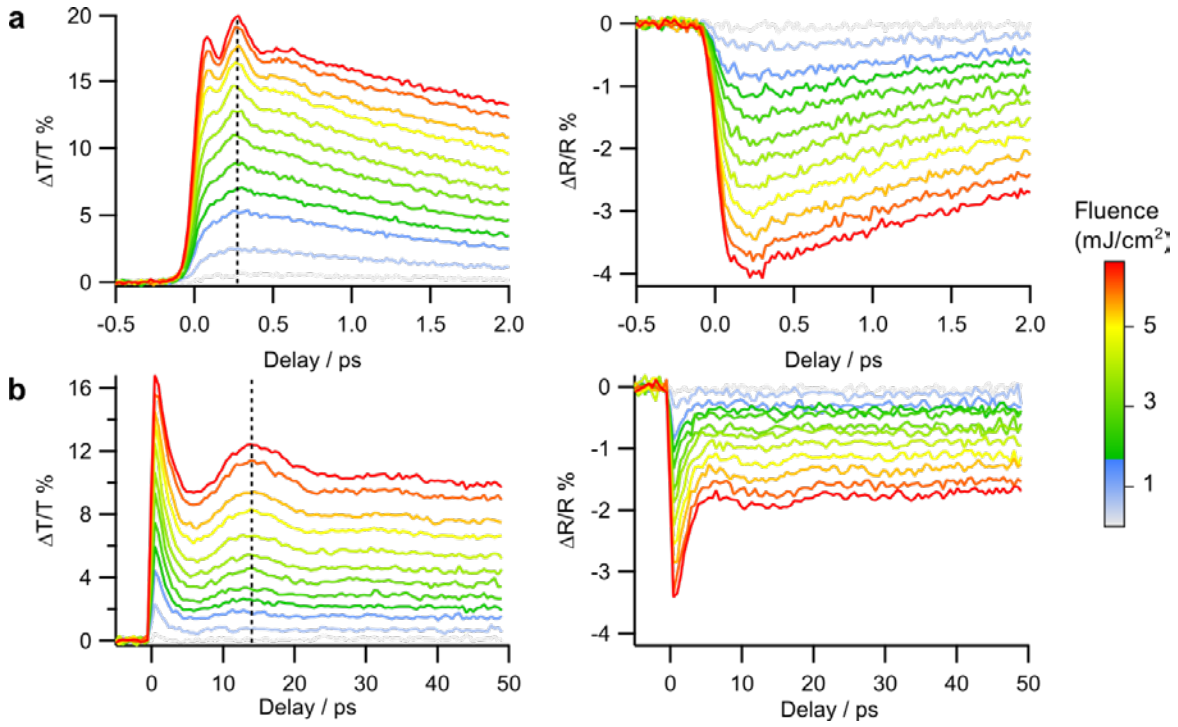

Figure S2 | Measured Reflectivity and Transmission of GST Films Used to Calculate the Time-Dependent Dielectric Function a, Short timescale dynamics **b,** long time dynamics. Dashed lines show the frequency independence of optical phonons (**a**) and acoustic phonons (**b**) on the pump fluence.

Below-threshold data

The optical data in Figure 2 of the manuscript is derived from the changes in reflectivity and transmissivity of the sample measured using conventional lock-in detection. Figure S2 shows both the data on short (a) and long (b) timescales used to extract the recovery time. On short timescales we observe coherent oscillations that can be attributed to coherent Raman-active phonons (see Figure S3); these predominantly influence the transmission. The dashed line marks the end of one oscillation period and indicates that the coherent phonon frequency remains constant for all pump fluences. On longer timescales we observe a slower oscillation corresponding to the breathing motion of the film, and the frequency is set by the speed of sound of the material. As the period of oscillation for both the optical and acoustic phonons remains constant, we conclude that there is no weakening of the lattice potential in this excitation regime.

Transfer Matrix Method

Reflection and transmission from a layered sample can be converted into the complex dielectric function using a transfer matrix method[8]. A general transfer matrix is written as:

$$T_n = \begin{pmatrix} \cos(2\pi n \delta/\lambda) & -\frac{i}{n}\sin(2\pi n \delta/\lambda) \\ -i\, n \sin(2\pi n \delta/\lambda) & \cos(2\pi n \delta/\lambda) \end{pmatrix} \qquad (1)$$

where n is the complex refractive index, δ is the layer thickness and λ is the wavelength of the light. The transmission, T, and reflection coefficient, R, for the multilayer system studied here can then be obtained from the combined system $T_{SiO_2} T_{GST} T_{Si_3N_4}$ with the light entering the Si_3N_4 layer from air and leaving the GST layer into the SiO_2

substrate. A small amount of light is further reflected from the SiO_2-air interface. This reflection is treated incoherently, i.e. light originating from multiple reflections inside the SiO_2 layer does not interfere.

The time dependent dielectric function is obtained by calculating T_{GST} for a range of complex refractive indices $n' = n + \Delta$, and the average is taken of the values of n' that satisfy both *R(t)* and *T(t)* simultaneously. From the resulting value for n' the dielectric function can be obtained. The same method is used for calculating the complex dielectric function above the amorphization threshold.

We fit the change in dielectric function with the following phenomenological model in the reversible regime:

$$\Delta\varepsilon = -Ae^{-\frac{t}{\tau}} - B\left(1 - e^{-\frac{t}{\tau}}\right), t > 0 \qquad (2)$$

where A and B are complex and τ is the recovery time of the optical signal (from Figure 1). The signal is then convolved with a Gaussian pulse of 40 fs FWHM to account for the experimental resolution. The results of the fit are shown in Figure S3 for the highest reversible fluence excitation, and an excellent fit is obtained. We attribute the A term to the dynamics of the resonantly bonded state. We can see that the dynamics of this term occur in both the real and imaginary part of the dielectric function. The coherent phonon signal, on the other hand, is only observed on the imaginary part of the dielectric function (i.e. the real part of B is small), and is in good agreement with the static Raman scattering signal.

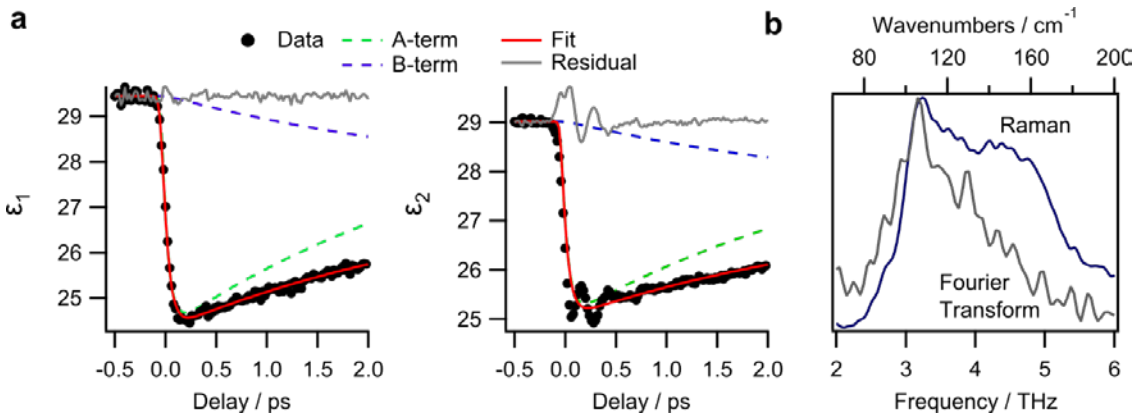

Figure S3 | Typical Fitting results for the broadband dielectric function a, shows the fit parameters for the two terms in Equation 2, together with the residual. **b,** The Fourier transform of the residual obtained from the imaginary part from **a**, compared to the static Raman measurement.

SINGLE-SHOT OPTICAL TECHNIQUE

The linear chirp imparted on the probe beam, generated by passing through a thick glass block, results in a time-dependent instantaneous frequency. The pump and probe beams are timed so that roughly 1/3 of the probe beam has passed through the sample before the pump beam arrives. As a result, each color in the beam experiences a different value of the transient refractive index of the sample. If we assume that the resulting ΔR/R and ΔT/T due to the time dependent dielectric function is independent of the probe frequency within our laser spectrum, we can extract the time-dependent signal.

The frequency-to-time calibration was achieved by using a motorized delay stage to change the relative arrival time between pump and probe beams. The time zero position was found by fitting an error function to the signal at each

DOI: 10.1038/NMAT4359

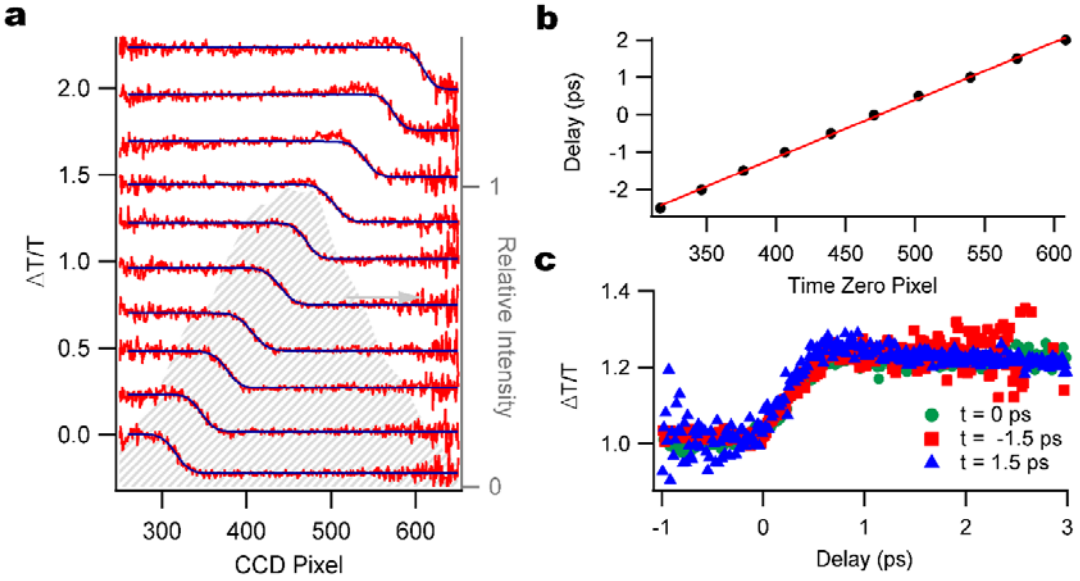

Figure S4 | Calibration of the spectral signal into the time domain a, The physical pump-probe delay is varied and the rising edge of the signal fit to an error function. The laser spectrum is shown in the background. **b,** The time zero point from (**a**) is plotted for different physical probe delays and shows the pulse has a linear chirp of 15.4 fs/px. **c,** The recorded dynamics are shown to be independent of wavelength within the measured spectral range. After shifting the time traces by the appropriate time delay, the exact same dynamics are observed. Note that the increased noise at negative delays for t=-1.5 ps and positive delays for 1.5ps is due to the loss of intensity at the edges of the spectrum.

delay as shown in Figure S4a. Figure S4b shows the extracted chirp of the pulse, which is 15.4 fs/pixel. Figure S4c shows that the ultrafast optical change of GST is independent of the probe wavelength. A limited spectral range was chosen for the dynamics due to the decrease in spectral intensity at the wings of the spectrum, resulting in more noise on the data.

To measure the irreversible dynamics we perform three measurements at each position on the sample. First, we measure a reflection (R_1) and transmission (T_1) spectrum of the sample when there is no pump beam. We then

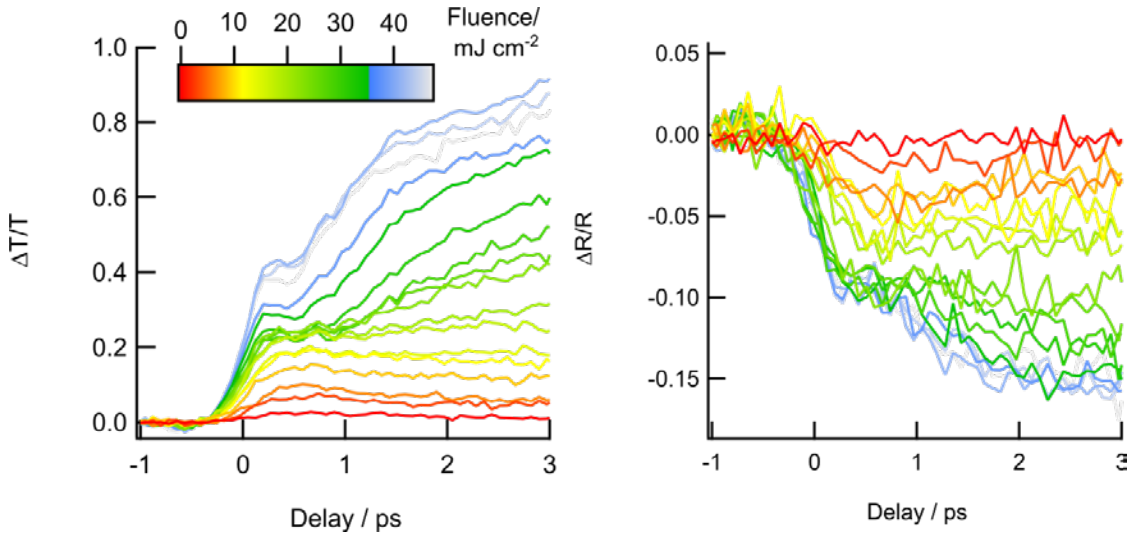

Figure S5 | Measured ΔT/T and ΔR/R Time Traces Using the Single Shot Technique

measure the same spectra (R_2 and T_2) when a pump beam excites the sample. The third measurement of the transmission and reflection spectra is again performed without the pump beam (R_3, T_3) to observe any permanent change. This process is repeated at 5 different points on the sample and then averaged. The permanent transmission change plotted in Figure 1d of the paper is obtained by averaging (T_3/T_1)-1 for each power. The dynamics of the reflectivity are obtained using $\Delta R/R = (R_2/R_1)$ -1 and the equivalent for $\Delta T/T$. These dynamics are shown in Figure S5 and are processed in the same way as the below-threshold data to calculate the dielectric function.

BIBLIOGRAPHY

1. Shportko, K. *et al.* Resonant bonding in crystalline phase-change materials. *Nat. Mater.* **7,** 653–8 (2008).

2. *Phase Change Materials - Science and Applications*. (Springer, 2009).

3. Park, J.-W. *et al.* Optical properties of pseudobinary GeTe, $Ge_2Sb_2Te_5$, $GeSb_2Te_4$, $GeSb_4Te_7$, and Sb_2Te_3 from ellipsometry and density functional theory. *Phys. Rev. B* **80,** 115209 (2009).

4. Němec, P. *et al.* Ge–Sb–Te thin films deposited by pulsed laser: An ellipsometry and Raman scattering spectroscopy study. *J. Appl. Phys.* **106,** 103509 (2009).

5. Hsieh, W.-P., Zalden, P., Wuttig, M., Lindenberg, A. M. & Mao, W. L. High-pressure Raman spectroscopy of phase change materials. *Appl. Phys. Lett.* **103,** 191908 (2013).

6. Němec, P. *et al.* Amorphous and crystallized Ge–Sb–Te thin films deposited by pulsed laser: Local structure using Raman scattering spectroscopy. *Mater. Chem. Phys.* **136,** 935–941 (2012).

7. Andrikopoulos, K. S., Yannopoulos, S. N., Kolobov, a. V., Fons, P. & Tominaga, J. Raman scattering study of GeTe and $Ge_2Sb_2Te_5$ phase-change materials. *J. Phys. Chem. Solids* **68,** 1074–1078 (2007).

8. Born, M. & Wolf, E. *Principles of Optics*. (Cambridge University Press, 2006).